

formation are abnormal temperature or salinity or proximity in the reproductive cycle to spawning.

Trace metals in the pollutants may also affect the concentrations of elements within the concretions. For example, zinc is known to be concentrated by the kidneys of some mollusks (16). High zinc contents in the concretions may be caused by relatively large amounts of zinc in industrial pollutants which are further concentrated by the organism.

Both *A. irradians* and *M. mercenaria* are widespread and common, and range from Nova Scotia to Florida in the Atlantic and from northern Florida to Texas in the Gulf of Mexico. *Argopecten irradians* is usually found in shallow coastal bays containing stands of eelgrass in the northern portions of its range or turtle grass in the southern portions. Populations of scallops fluctuate widely from year to year and location to location, although we have observed densities as great as 22 per square meter. *Mercenaria mercenaria* is found in muddy sediments in coastal waters. Populations of these animals also fluctuate widely, but the densities are often high enough for commercial exploitation. The extensive range and high densities of mollusks suggest that biogenic phosphorite could be deposited in many marine environments. The fact that the same or similar species also extend far back into the geologic past suggests that this process may have been active in earlier times.

Concretions may be incorporated into the sediment when the animal dies either as a result of old age or as a result of renal failure. Some concretions may be excreted from the living animal, since we have observed them in tissue sections in the vicinity of the renal pore. Long periods of time as well as secondary enrichment (suggested by the small weights of phosphorite concretions in 400 animals) and diagenetic change from an amorphous to crystalline structure may be required to form biogenic phosphorite deposits.

Irrefragable evidence of direct biogenic formation of phosphorite has profound consequences. Its deposition is restricted only by range constraints on the organisms involved and does not require the special oceanographic conditions that chemical formation of phosphorite does. Biogenic formation of phosphorite does not rule out chemical or diagenetic formation, either in the past or the present. However, if biogenic phosphorite is preserved in sediments, it may explain deposits that do not seem to fit the chemical precipitation-replacement hypotheses such as those that have been

suggested to account for the formation of the continental margin of the Southeast where the phosphorite is distributed throughout the sediments as discrete sand-sized or smaller grains.

LARRY J. DOYLE

NORMAN J. BLAKE

Department of Marine Science,
University of South Florida,
St. Petersburg 33701

C. C. WOO

U.S. Geological Survey,
Woods Hole, Massachusetts 02543

PAUL YEVICH

Environmental Protection
Agency Laboratory,
Narragansett, Rhode Island 02882

References and Notes

1. A. V. Kazakov, *Trans. Inst. Fert. Insectofung. (U.S.S.R.)* **142**, 93 (1937), as cited in Kolodny (6).
2. H. H. Veeh, W. C. Burnett, A. Soutar, *Science* **181**, 844 (1973).
3. F. Manheim, G. T. Rowe, D. Jipa, *J. Sediment. Petrol.* **45**, 243 (1975).
4. B. F. D'Anglejan, *Can. J. Earth Sci.* **5**, 81 (1967).

5. W. C. Burnett, *Geol. Soc. Am. Bull.* **88**, 813 (1977).
6. Y. Kolodny, *Nature (London)* **224**, 1017 (1969).
7. K. O. Emery, *The Sea Off Southern California* (Wiley, New York, 1960); D. Pasho, thesis, University of Southern California (1973).
8. G. N. Baturin, K. I. Merkulove, P. I. Chalove, *Mar. Geol.* **13**, M37 (1972).
9. W. C. Burnett and H. H. Veeh, *Geochim. Cosmochim. Acta* **41**, 775 (1977).
10. B. F. D'Anglejan, *Mar. Geol.* **5**, 15 (1967).
11. D. McConnell, *Geol. Soc. Am. Bull.* **74**, 363 (1963); J. D. Milliman, *Marine Carbonates* (Springer-Verlag, New York, 1974).
12. D. McConnell, *Apatite* (Springer-Verlag, New York, 1973).
13. R. L. McMaster, *J. Sediment. Petrol.* **30**, 401 (1960); *ibid.* **32**, 484 (1962).
14. K. M. Towe, *ibid.* **29**, 503 (1959).
15. M. Krahelska, *Z. Naturwiss. Jena* **46**, 363 (1910); J. Strohl in *Handbuch der Vergleichenden Physiologie*, H. Winterstein, Ed. (Fisher, Jena, 1924), p. 143; J. Bouillon, *Ann. Sci. Nat. Zool. Biol. Anim.* **12** (ser. 2), 719 (1960); W. T. W. Potts, *Biol. Rev. City Coll. N.Y.* **42**, 1 (1967).
16. G. W. Bryan, in *Marine Pollution*, R. Johnston, Ed. (Academic Press, New York, 1976), p. 219.
17. We thank D. Bankston who carried out the analyses summarized in Table 1, N. Thayer who collected the sediment samples, and F. T. Manheim who criticized the manuscript. We thank R. Rheinberger who extracted the concretions from *Mercenaria*, D. Johnson who arranged for SEM analyses of tissue sections at the N. C. Brown Laboratory for Ultrastructure Analysis, and J. McLane who provided assistance during SEM analysis of the sperules.

3 June 1977; revised 28 November 1977

Imbrian-Age Highland Volcanism on the Moon: The Gruithuisen and Mairan Domes

Abstract. *The Gruithuisen and Mairan domes on the moon represent morphologically and spectrally distinct nonmare extrusive volcanic features of Imbrian age. The composition, morphology, and age relationships of the domes indicate that nonmare extrusive volcanism in the northern Procellarum region of the moon continued until about 3.3×10^9 to 3.6×10^9 years ago and was partially contemporaneous with the emplacement of the main sequence of mare deposits.*

The lunar maria and highlands show major differences in morphology, petrology, geochemistry, thermal history, and age (1). With few exceptions (2), these differences are viewed in terms of two distinct periods of lunar history with little or no overlap: an early period of highland crustal formation, volcanic activity, and bombardment, culminating in the formation of the Imbrium and Orientale basins, followed by a period characterized by the extrusion of mare lavas and less intense bombardment. There is some evidence, however, for the continued emplacement of nonmare volcanic geologic units during the period of mare volcanism. We have obtained spectra and vidicon imagery of several such regions and compiled detailed geologic maps in order to (i) characterize these anomalous areas compositionally and compare them to returned samples and to other mare and highland regions, and (ii) establish age relationships and mode of origin. We report here geologic and spectral evidence for the extensive overlap in time of mare volcanism and a dis-

tinctive nonmare surface unit apparently of extrusive volcanic origin.

A series of domical features located near the shores of northeastern Oceanus Procellarum adjacent to Iridum crater (Fig. 1) have long attracted attention because of their relatively high albedo and morphological distinctiveness. The domes are very bright (red) in infrared-ultraviolet color-differenced photographs (3). Several additional "red spots" occur in a variety of geologic environments in the western portion of the lunar near side (4, 5). In this report we concentrate on one of the red spot areas, the Gruithuisen domes, and an adjacent area with similar characteristics (Fig. 1, a through c).

Recently, McCord *et al.* obtained digital images at several wavelengths, using a silicon vidicon imaging system and earth-based telescopes (6). The photometric precision of these images is at least 1 percent, and the spatial resolution is about 2 km at the subearth point. We have prepared ratio images for the region of Fig. 1a by dividing images obtained at

two wavelengths (0.40/0.56 μm and 0.95/0.56 μm). None of the domes can be distinguished on the 0.95/0.56- μm images. However, they appear very distinctive on the 0.40/0.56- μm images (Fig. 1, d and e). The very dark regions in Fig. 1, d and e, closely correspond to the Mairan and Gruithuisen domes and are very distinct from the background mare and highland materials.

The domes are topographically distinct from adjacent highland and mare terrain and also show unique surface morphology. The domes considered here generally stand hundreds of meters higher than the adjacent topography (Fig. 1, b and c). Most of the domes are roughly circular in outline, although the largest dome, Gruithuisen δ , is rectangular and may be composed of several coalescing

domes. The Mairan domes are generally smaller in both diameter and elevation than the Gruithuisen domes, although mare flooding at the Mairan domes may contribute to reduced size estimates. Mairan T is circular, about 6 to 7 km in diameter, over 900 m high, and its crest is made up of several coalescing craters. Although several domes have distinct craters on their surfaces, most such features appear to be superposed impact craters in view of their relative freshness, ray systems, and raised rims. However, the series of craters on Mairan T may be of internal origin. Gruithuisen γ is roughly circular, averages about 20 km in diameter, and is over 1200 m high. Its broad flat top is typical of several of the domes. Slopes on the dome flanks range from 15° to 30°, although on the flanks of Mairan T they may be as high as 35°.

High-resolution imagery of Gruithui-

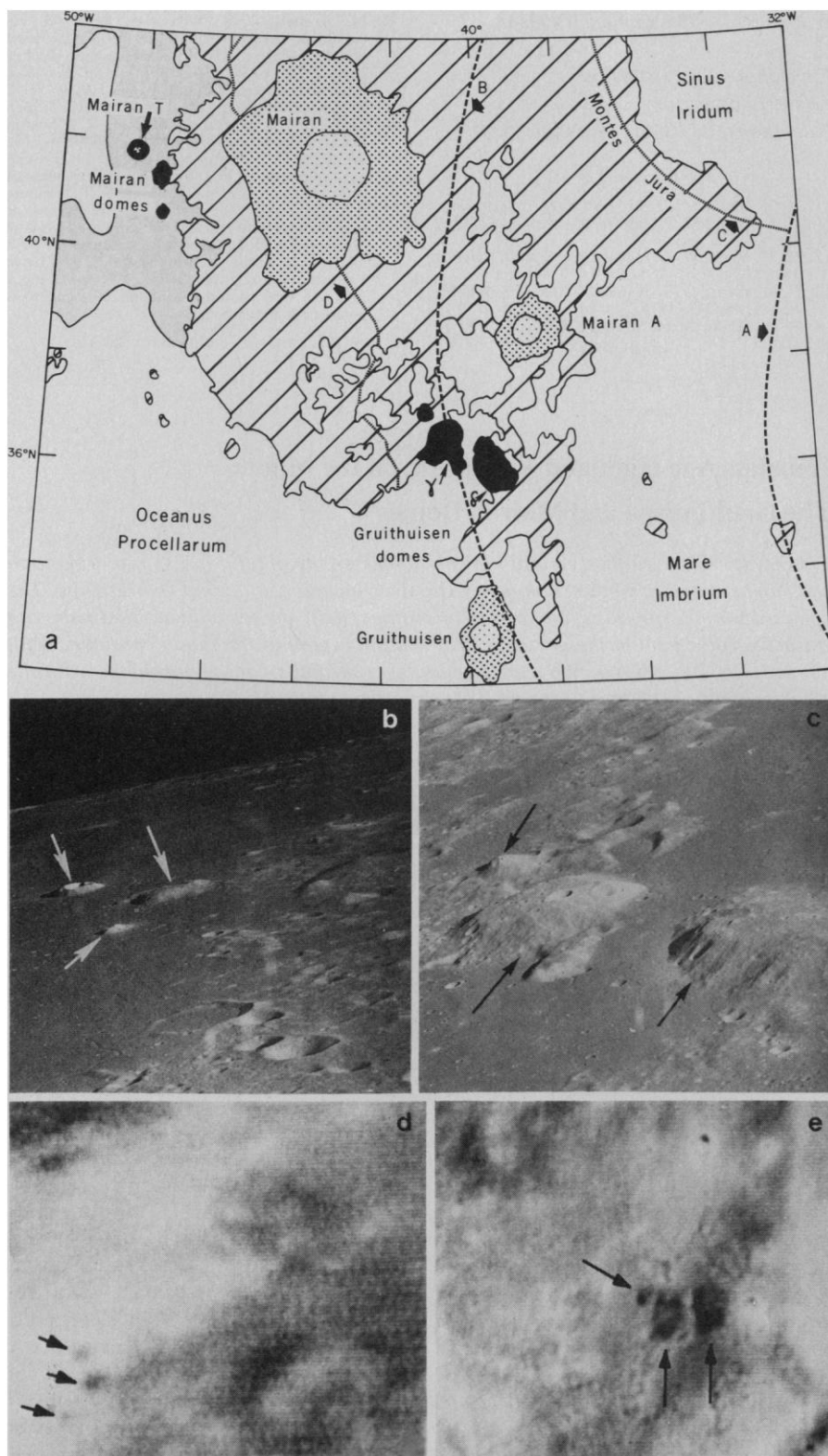


Fig. 1. (a) Location and geologic setting of the Gruithuisen and Mairan domes (black). Two rings of the Imbrium multiringed basin pass through the area: A marks the location of the inner, or peak ring; B marks the location of the second, or intermediate ring, equivalent to the Montes Alpes ring in eastern Imbrium. Montes Jura (C) mark the rim crest of the Imbrian-aged Iridum crater. Lined areas are highland terrain dominated primarily by Iridum ejecta deposits. Line D separates areas of radially textured Iridum rim material (toward Montes Jura) and the regions dominated by Iridum secondary craters (southwest of the line). Mare units (plain) flood and surround the uplands, and are mostly of Imbrian age. Eratosthenian units surrounding the Mairan domes are indicated in gray. Large craters and associated deposits are of various ages (Mairan, Imbrian; Gruithuisen, Eratosthenian; Mairan A, Copernican). Most geologic unit boundaries are summarized from (10, 13). One degree of latitude equals approximately 30 km. (b) The Mairan domes (indicated by arrows). The left arrow is Mairan T, approximately 6 to 7 km in diameter and over 900 m high. The dome indicated by the right arrow averages about 11 to 12 km in diameter and is 500 to 600 m in elevation; the small dome indicated by the central arrow is elongate, less than 5 km in its longest dimension, and between 400 and 500 m in height (Apollo 15 image AS15-12730). (c) The Gruithuisen domes (indicated by arrows). The upper left arrow indicates the dome northwest of Gruithuisen γ which is roughly circular, averaging about 8 km in diameter and 1100 m in elevation. The central arrow points to the base of Gruithuisen δ , a flat-topped dome averaging about 20 km in diameter and over 1200 m in height. A grooved and furrowed portion of the dome flank occurs just above the arrow. Gruithuisen δ (right arrow) is rectangular (about 13 by 33 km), flat-topped, and 1500 to 1600 m in height (Apollo 15 image AS15-12718; the view is toward the north). (d) Color-difference image of the Mairan dome region at 0.40/0.56 μm . Domes are indicated by arrows. (e) Color-difference image of the Gruithuisen dome region at 0.40/0.56 μm . Domes are indicated by arrows.

sen γ shows a broad flat top with areas of rough and relatively smooth texture, sinuous scarps (predominantly in the smooth-textured unit), and an occasional smaller summit dome 1 to 2 km in diameter. The flanks of Gruithuisen γ are characterized by a very distinctive texture quite dissimilar to that observed on normal highlands or crater slopes and consisting of ridges and furrows generally oriented downslope. The slope texture is well developed locally along the flanks of Gruithuisen γ where two distinct units appear to originate in the smooth crest unit and extend into adjacent highlands to the southeast and to be embayed by the mare at the base of the dome to the south (to the left of and above the middle arrow in Fig. 1c). Both of these units appear to be large flows or a series of flows, which originated from the crest of the dome and extended down the flanks and out onto adjacent terrain.

The morphological and the textural uniqueness of these domes is further emphasized by comparison with lunar mare domes of volcanic origin. Analysis of 47 domes associated with mare basalts shows that they have the following general characteristics relative to the domes under consideration: (i) lower albedo (comparable to that of the surrounding mare), (ii) smaller diameter range (3 to 16

km), (iii) much smaller heights (average less than 200 m), (iv) smooth surface texture, and (v) abundant summit pits of apparent volcanic origin (7). Lunar mare domes are generally analogous in size, morphology, and apparent eruption conditions to small shield volcanoes typical of terrestrial basaltic plains (7). The Gruithuisen and Mairan domes are similar in shape and surface texture to many terrestrial domes of dacitic and rhyolitic composition characterized by extrusions of more viscous lavas at low rates. However, the scale is considerably different. Measurement of 36 domes in the Mono Lake and Coso Hills region of California showed maximum dimensions of 2 km in width and 250 m in height. In summary, the Gruithuisen and Mairan domes appear morphologically and texturally distinct from the surrounding mare materials and show no obvious affinities with background highland topography. The morphology and surface texture suggest a volcanic origin for the domes, distinct from mare basalt eruption styles, and comparable to styles typical of more acidic terrestrial compositions.

The Gruithuisen domes are prominent in color-difference images obtained at 0.40/0.56 μm but not in those obtained at 0.95/0.56 μm (Fig. 1, d and e). An inspection of the relative reflectance spec-

trum for these lunar surface features [Fig. 2, a(1)] reveals the strong ultraviolet absorption responsible for the red color. Other reflectance spectra [Fig. 2, a(1) and a(2)] demonstrate the existence of additional regions of lunar surface material of high albedo which have similar spectral reflectance properties. These characteristic red spot spectra differ from the usual spectra of mature upland regions in this spectral range only in the strong ultraviolet absorption (Fig. 2b). No known mare area spectra are similar to the red spot spectra (8). Thus, the Gruithuisen domes are spectrally distinct from the surrounding highland and mare material but are quite similar in a distinctive way to other areas of high albedo on the western lunar near side known as red spots (4, 5).

There is abundant evidence that spectral characteristics, and in particular absorption in the reflectance spectrum of lunar rocks and soils, whether viewed through the telescope or in the laboratory, are controlled by the mineralogical composition of the reflecting material. Thus, the spectral distinctiveness of the red spots implies a mineralogical distinctiveness from surrounding materials. The spectra indicate that the red spot areas are covered with mature (agglutinate-rich) soils with a lower content of

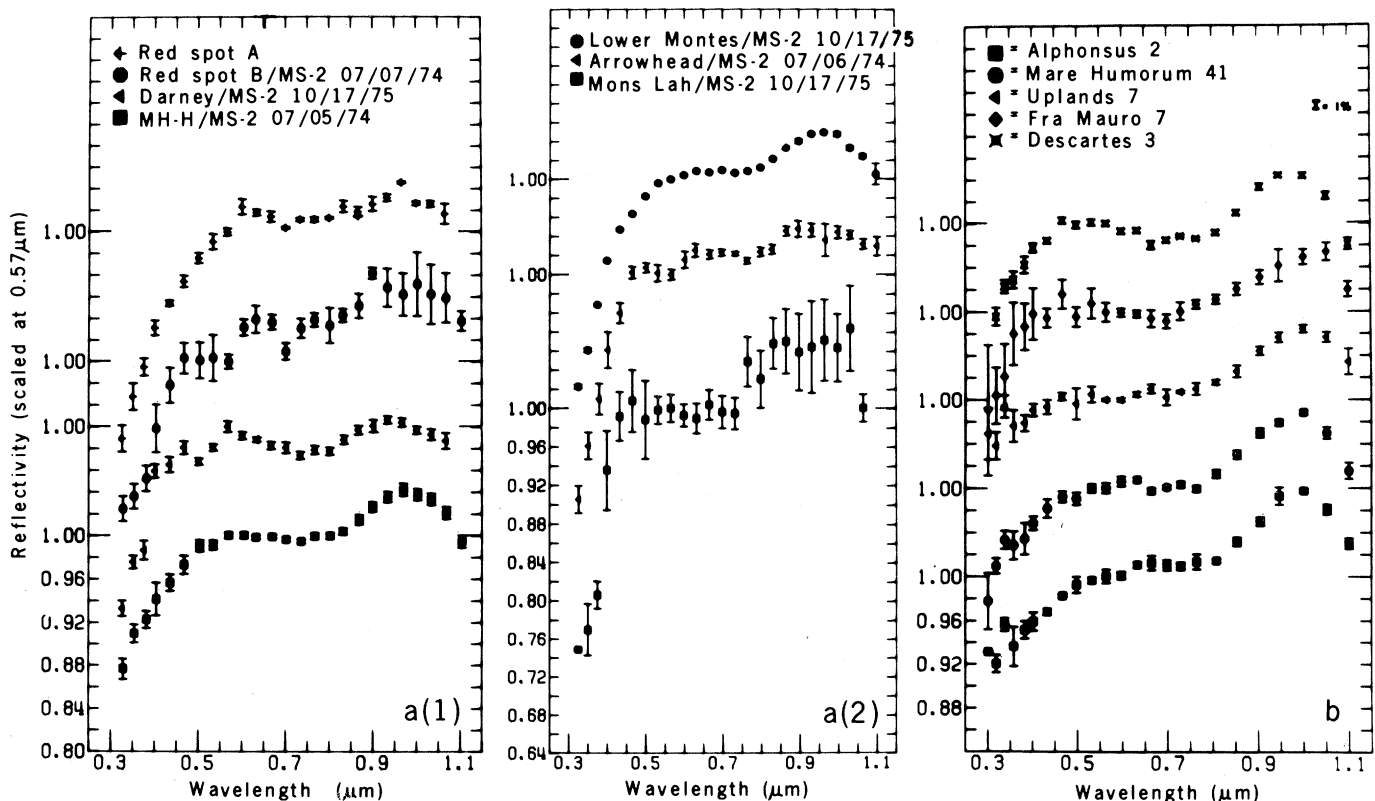


Fig. 2. [a(1) and a(2)] The relative reflectance spectra of seven lunar areas with "red spot" characteristics (12), including red spot A (which corresponds to Gruithuisen γ) and B (Gruithuisen δ). The relative reflectance is derived by dividing the reflectance spectra by the reflectance spectrum of a standard area in Mare Serenitatis (MS-2) and scaling the result to unity at 0.56 μm (8); MH-H, Mare Humorum-Helmet. (b) Relative reflectance spectra for normal mature lunar upland regions, which are distinctive from red spot spectra.

iron and titanium than mare soils, and perhaps lower than most highland soils. However, the specific compositional property causing the ultraviolet absorption in the red spot spectra is unknown. Correlations of red spots and KREEP (potassium, rare-earth elements, phosphorus) basalts have been suggested (4). However, preliminary analyses of laboratory spectra have not yet established any correlation with specific types of highland basalts (9).

Evidence from several sources demonstrates an Imbrian age for the domes. Stratigraphic relationships (Fig. 1a) show the domes to be superposed on the Imbrium basin and to postdate the formation of Iridum crater, of middle Imbrian age (10). Mare basalts mapped as Imbrian embay the Gruithuisen domes, and Eratosthenian mare (10) surrounds the Mairan domes. Techniques for dating crater morphology suggest an age of 3.1×10^9 to 3.3×10^9 years for the mare surrounding the two dome areas (11). On the basis of available evidence, the domes appear to have formed in middle Imbrian time, most likely between 3.3×10^9 and 3.6×10^9 years ago.

In conclusion, geologic and spectral reflectance evidence shows that a distinctive style of extrusive nonmare volcanism in northeastern Procellarum extended for perhaps 0.5×10^9 years into the period of mare volcanism. Several areas with similar spectral characteristics are known in the Oceanus Procellarum region and occur in a variety of geologic environments that may be synchronous with or predate the Mairan and Gruithuisen domes (4, 5). Vidicon images and spectra for these regions have been obtained to document the characteristics, composition, and mode of emplacement of these distinctive geologic occurrences (12).

JAMES W. HEAD III

Department of Geological
Sciences, Brown University,
Providence, Rhode Island 02912

THOMAS B. MCCORD

Institute for Astronomy,
University of Hawaii, Honolulu 96821

References and Notes

1. S. R. Taylor, *Lunar Science: A Post Apollo View* (Pergamon, New York, 1975); J. W. Head, *Rev. Geophys. Space Phys.* **14**, 265 (1976); D. Wilhelms and J. McCauley, *U.S. Geol. Surv. Geol. Atlas Moon I-703* (1971).
2. G. Taylor and G. Ryder, *Geochim. Cosmochim. Acta* **2** (Suppl. 7), 1741 (1976).
3. E. Whitaker, in *The Nature of the Lunar Surface*, W. Hess, D. Menzel, J. O'Keefe, Eds. (Johns Hopkins Press, Baltimore, 1966), p. 79.
4. M. Malin, *Earth Planet. Sci. Lett.* **21**, 331 (1974).
5. C. Wood and J. Head, *Origins of Mare Basalts* (Lunar Science Inst., Houston, 1975), p. 189.
6. T. McCord, C. Pieters, M. Feierberg, *Icarus* **29**, 1 (1976).
7. J. Head and A. Gifford, *Moon*, in press.

8. T. McCord, M. Charette, T. Johnson, L. Lebofsky, C. Pieters, *J. Geophys. Res.* **77**, 1349 (1972).
9. J. Adams, personal communication.
10. D. Scott and R. Eggleton, *U.S. Geol. Surv. Geol. Atlas Moon I-805* (1973).
11. J. Boyce, *Geochim. Cosmochim. Acta* **3** (Suppl. 7), 2717 (1976).
12. J. Head and T. McCord, in preparation.
13. G. Schaber, *U.S. Geol. Surv. Geol. Atlas Moon I-602* (1969).

14. Thanks are extended to M. Settle, M. Cintala, C. Wood, B. R. Hawke, and J. Whitford-Stark for reviews and to N. Christy, S. Bosworth, and W. Rhea for help in the compilation of the manuscript. This work was supported under NASA grants NSG-7048 (T.B.M.) and NGR-40-002-116 (J.W.H.). Publication 179 of the Remote Sensing Laboratory, Institute of Astronomy, University of Hawaii.

6 October 1977; revised 9 January 1978

Salt Domes: Is There More Energy Available from Their Salt than from Their Oil?

Abstract. Calculations indicate that a typical oil-bearing salt dome along the Gulf Coast of the United States contains more energy in its salt than is present in its oil. The magnitude of the potential salinity gradient energy is even greater when all of the salt domes are considered.

At the interface between salt solutions of different concentrations, there is a potentially large source of usable energy. It is manifest mechanically in terms of the osmotic pressure difference between the two solutions. For the case of freshwater versus seawater, such as at a location where a river flows into the ocean, the osmotic pressure difference equals about 24 atm (1), equivalent to the pressure at the bottom of a column of water 240 m (750 feet) high. This height is comparable to the highest dams in existence. The energy inherent in this system is such that river water flowing at the rate of 1 m^3 per second theoretically represents more than 2 MW of power as it mixes with the sea.

The energy density is even higher where freshwater flows into a hypersaline lake such as the Dead Sea or the Great Salt Lake. The osmotic pressure difference is as high as 500 atm for the Dead Sea (2) (because of the large amount of the divalent salt MgCl_2 in the brines) and about 370 atm for the Great Salt Lake. In these cases the power can be greater than 30 MW for each cubic

meter per second of fresh water flowing into the hypersaline lake.

There are other likely sources of salinity gradient energy. Along arid and semi-arid coasts, dried lagoons or salt pans exist. Controlled influx of seawater will create concentrated brines that can be interfaced with seawater serving as the dilute solution. Subterranean brines and salt deposits can also be utilized as long as there is sufficient water, either fresh or brackish or marine, to form the dilute solution.

Several schemes have been suggested to harness salinity gradient energy (3, 4). They range from mechanical conversion based on the use of the osmotic pressure difference or the vapor pressure difference of the two solutions, through electrical conversion by means of reverse electro dialysis, as in a dialytic battery. However, further research and development are necessary before any of these schemes can be actualized. All of the proposed methods will operate in principle between any two salt solutions with different concentrations.

Salt domes, subterranean formations

Table 1. Comparison of the energy available from the salt and the oil in selected salt domes (7).

Dome	Salt volume (cubic miles)	Oil production (10^9 barrels)	Salt energy (MW-years)	Oil energy (MW-years)
<i>High yield</i>				
Thompson (Ft. Bend, Texas)	0.4	259,623	14,000	44,000
Hull (Liberty, Texas)	2.6	156,830	93,000	27,000
Humble (Harris, Texas)	9.8	138,639	350,000	24,000
<i>Medium yield</i>				
Avery Island (Iberia, La.)	4.0	53,054	140,000	9,000
Bayou Blue (Iberville, La.)	4.6	20,806	161,000	3,500
Belle Isle (St. Mary, La.)	1.9	10,316	68,000	1,700
<i>Low yield</i>				
Lake Hermitage (Plaquemines, La.)	0.9	2,475	32,000	420
Bethel (Anderson, Texas)	8.0	1,017	280,000	172
East Tyler (Smith, Texas)	4.3	55	150,000	9